



HAL
open science

Aptamer-based liposomes improve specific drug loading and release

Kevin Plourde, Rabeb Mouna Derbali, Arnaud Desrosiers, Céline Dubath, Alexis Vallée-Bélisle, Jeanne Leblond

► **To cite this version:**

Kevin Plourde, Rabeb Mouna Derbali, Arnaud Desrosiers, Céline Dubath, Alexis Vallée-Bélisle, et al.. Aptamer-based liposomes improve specific drug loading and release. *Journal of Controlled Release*, 2017, 10.1016/j.jconrel.2017.02.026 . hal-02512401

HAL Id: hal-02512401

<https://hal.science/hal-02512401v1>

Submitted on 23 Mar 2020

HAL is a multi-disciplinary open access archive for the deposit and dissemination of scientific research documents, whether they are published or not. The documents may come from teaching and research institutions in France or abroad, or from public or private research centers.

L'archive ouverte pluridisciplinaire **HAL**, est destinée au dépôt et à la diffusion de documents scientifiques de niveau recherche, publiés ou non, émanant des établissements d'enseignement et de recherche français ou étrangers, des laboratoires publics ou privés.

1 Aptamer-based liposomes improve specific drug loading and release

2 Kevin Plourde¹, Rabeb Mouna Derbali¹, Arnaud Desrosiers², Céline Dubath¹, Alexis Vallée-
3 Bélisle², Jeanne Leblond¹

4 ¹ Faculty of Pharmacy, ² Department of Chemistry, University of Montreal, QC, Canada H3T 1J4

5 Corresponding author: Jeanne Leblond, PO Box 6128, Downtown station, Montréal, QC, H3C
6 3J7, Canada, Jeanne.leblond-chain@umontreal.ca

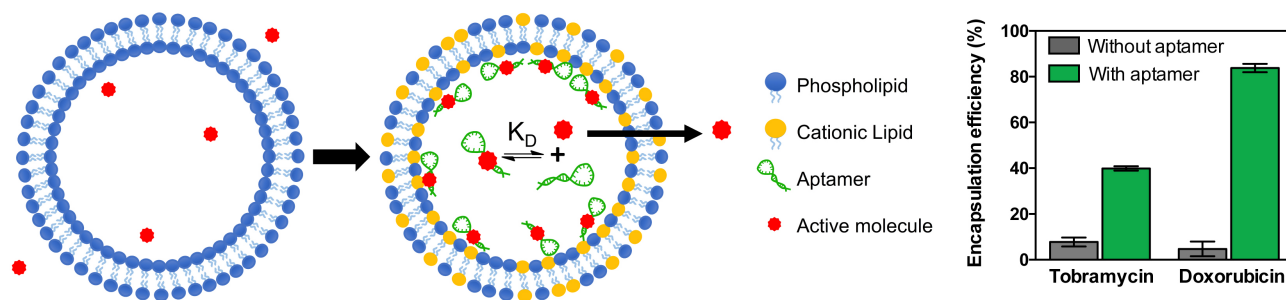
7 **Abstract**

8 Aptamer technology has shown much promise in cancer therapeutics for its targeting abilities.
9 However, its potential to improve drug loading and release from nanocarriers has not been
10 thoroughly explored. In this study, we employed drug-binding aptamers to actively load drugs into
11 liposomes. We designed a series of DNA aptamer sequences specific to doxorubicin, displaying
12 multiple binding sites and various binding affinities. The binding ability of aptamers was preserved
13 when incorporated into cationic liposomes, binding up to 15 equivalents of doxorubicin per
14 aptamer, therefore drawing the drug into liposomes. Optimization of the charge and drug/aptamer
15 ratios resulted in $\geq 80\%$ encapsulation efficiency of doxorubicin, ten times higher than classical
16 passively-encapsulating liposomal formulations and similar to a pH-gradient active loading
17 strategy. In addition, kinetic release profiles and cytotoxicity assay on HeLa cells demonstrated
18 that the release and therapeutic efficacy of liposomal doxorubicin could be controlled by the
19 aptamer's structure. Our results suggest that the aptamer exhibiting a specific intermediate affinity
20 is the best suited to achieve high drug loading while maintaining efficient drug release and
21 therapeutic activity. This strategy was then successfully applied to tobramycin, a hydrophilic drug

22 suffering from low encapsulation into liposomes, where its loading was improved six-fold using
23 aptamers. Overall, we demonstrate that aptamers could act, in addition to their targeting properties,
24 as multifunctional excipients for liposomal formulations.

25 **Keywords:** liposome, aptamer, doxorubicin, encapsulation efficiency, controlled release, active
26 loading

27 Graphical abstract



28

29

30 **Introduction**

31 Aptamer technology, although discovered for 25 years, is still evolving to fulfill the requirements
32 of more precise diagnosis and personalized therapy [1, 2]. Aptamers are RNA or DNA sequences
33 generated to exhibit high affinity and specificity against a broad range of targets, ranging from
34 small molecules to whole cells or tissues [2-4]. Like antibodies, they recognize their specific
35 targets due to the unique three-dimensional structure they adopt. Nucleotide aptamers, however,
36 exhibit several improved properties when compared to antibodies, such as lower immunogenicity,
37 higher thermal stability, rapid and large-scale synthesis and lower production costs [5, 6]. To date,
38 they have shown a high potential for clinical translation, especially in the field of drug and
39 biomarker discovery [7, 8], biosensor design [9, 10], vaccines [11] and molecular imaging [12,
40 13].

41 The pioneering work of Farokhzad *et al.* first demonstrated the potential of conjugating an aptamer
42 to the surface of polymeric nanoparticles for targeting prostate cancers *in vivo* [14]. Since then,
43 aptamers have been conjugated to multiple nanocarriers to provide specific recognition of
44 biological targets, showing much promise in targeted cancer therapeutics [15, 16]. However,
45 loading sufficient therapeutics into nanocarriers, while controlling its release rate in order to reach
46 therapeutic concentrations at the target site, still remains a major limitation of nanocarriers [17-
47 19]. Liposomes, for instance, offer unique benefits for clinical applications, such as large internal
48 volume for high drug loading, prolonged circulation times and controlled biodistribution, as well
49 as excellent biocompatibility and biodegradability [20]. To improve drug loading capacity, current
50 strategies exploit a trans-membrane gradient, such as pH- or ion- gradient, to actively load and
51 retain the drug into the liposomal core [21]. The most successful example is Doxil, commercialized

52 liposomes of doxorubicin, able to reach up to 10 000 molecules of doxorubicin per liposome, most
53 of which existing in the crystalline phase [21]. The liposome formulation significantly reduced the
54 cardiotoxicity of doxorubicin, but the strong entrapment of the drug within the core significantly
55 reduced its release, and, by extension, its therapeutic efficacy [22]. In extreme cases, such as
56 liposomal cisplatin, the therapeutic efficacy has even been abolished [23]. Alternative methods are
57 therefore pursued to provide a better control over the loading and release of the encapsulated drug
58 [24]. Recent studies have used ATP-binding aptamers to selectively release doxorubicin in an
59 ATP-rich environment from nanogels [25, 26], graphene nanosheets [27] or cross-linked
60 microcapsules [28]. Aptamer-functionalized hydrogels have also been programmed to release
61 various and multiple therapeutics when needed through specific nucleic acid recognition and
62 complementary hybridization process [29, 30].

63 In this study, we propose to use drug-specific aptamers to improve drug loading into liposomes.
64 Indeed, specific aptamers have been designed to show a tunable affinity for a variety of drugs such
65 as doxorubicin [31] [32], cocaine [33] or neomycin [34]. Interestingly, the loading and release rate
66 of the drug from aptamer-drug complexes is a function of the sequence [32, 34] and the number of
67 binding sites [31]. However, these complexes suffer from a low stability in the blood, limited drug
68 loading capacity and some inherent immunogenicity of the aptamers [15, 35]. We hypothesize that
69 incorporating the drug-aptamer complex into liposomes will improve specific drug loading and
70 offer a better control over the release rate to improve the therapeutic efficiency. We have designed
71 specific aptamer sequences to tune the binding affinity of doxorubicin and incorporated them into
72 liposomal formulations. The impact on drug loading, drug release and therapeutic efficacy was
73 investigated. This proof-of-concept was first demonstrated with doxorubicin and applied to
74 tobramycin, a hydrophilic drug suffering from low encapsulation into liposomes.

75 **Material and methods**

76 2.1 Chemicals and material

77 All lipids were purchased from Avanti Polar Lipids (Alabaster, AL). DNA aptamers and control
78 nucleotide sequences were purchased from Sigma-Aldrich custom oligonucleotide synthesis
79 service (Oakville, ON). The sequences are detailed in Table S1. Doxorubicin hydrochloride was
80 purchased from Sigma-Aldrich and tobramycin sulphate was purchased from AK Scientific (CA,
81 USA). EMEM (ATCC[®] 30-2003[™]), PBS and TrypLE Express was purchased from GE
82 Healthcare (Baie-d'Urfé, QC). All sterile consumables were purchased from Sarstedt (Montreal,
83 QC). All reagents, solvents and salts were either purchased from Sigma-Aldrich (Oakville, ON) or
84 Fisher Scientific (Whitby, ON). HeLa cells (ATCC[®] CCL-2[™]) were kindly provided by Prof.
85 Marc Servant (University of Montreal).

86 2.2 Dissociation constants of aptamer-doxorubicin complexes

87 Dissociation constants for the different aptamer-doxorubicin complexes were obtained by
88 monitoring the quenching of doxorubicin fluorescence at various aptamer concentrations. DNA
89 aptamer solution (0.1 mM in a solution of 5% dextrose and 5 mM NaCl) was denatured 5 minutes
90 at 95 °C, vortexed for 1 minute and annealed at room temperature. Doxorubicin sample
91 concentration was kept constant in all samples (100 nM in 5% dextrose and 5 mM NaCl).
92 Fluorescence emission spectrum (λ_{ex} 485 nm, λ_{em} 520-700 nm) was recorded at 37 °C on a Cary
93 Eclipse Fluorescence spectrophotometer (Agilent Technologies, Mississauga, ON). Increasing
94 amounts of DNA were added and equilibrated 1 minute at 37 °C in the same cuvette, producing
95 DNA concentrations ranging from 0.001 to 25 μM with incrementing volumes less than 20% of
96 final volume. Emission scans were taken at a high resolution of 100 nm/min and data were

97 smoothed with a 10-neighbors Savitzky-Golay factor. The area under curve of the full scan was
98 considered for the analysis. The dissociation constant (K_D , nM) was calculated using GraphPad
99 Prism 6 with the equation $Y=M_1 + (M_2*X)/(X+M_3)$, where M_1 is the initial value of Y, M_2 is its
100 magnitude and M_3 is the K_D . In the definition of Poly-Doxapt concentrations, one strand A
101 complexed with one strand A' was considered as one aptamer molecule (two binding sites).

102 2.3 Preparation and characterisation of liposomes

103 All liposome formulations, except Doxil-Like, were prepared using the hydration method. Briefly,
104 stock solutions of lipids in chloroform (20-40 mg/mL) were stored under argon at -80 °C before
105 use. For the preparation of cationic liposomes, 1,2-dioleoyl-3-trimethylammonium-propane
106 (DOTAP), cholesterol and 1,2-distearoyl-*sn*-glycero-3-phosphoethanolamine-N-(polyethylene
107 glycol)-2000 (DSPE-PEG₂₀₀₀) solutions were combined in a 10-mL round bottom flask in a
108 50/48/2 molar ratio to get 30 μ mol total lipid amount. The solvent was evaporated under reduced
109 pressure at 50 °C. The dried lipid film was hydrated 30 minutes at 60 rpm with 1 mL of 5%
110 dextrose and 5 mM NaCl. “No cationic lipid” formulation consisted in 1-palmitoyl-2-oleoyl-*sn*-
111 glycero-3-phosphocholine (POPC), cholesterol and DSPE-PEG₂₀₀₀ in a 55/40/5 molar ratio. All
112 liposomes were extruded through 400 and 200 nm polycarbonate membranes using a LiposoFast
113 manual extruder (Avestin Inc., Ottawa, ON, Canada) at room temperature. Doxil-Like liposomes
114 were prepared following the same procedure with minor modifications. Lipid composition was
115 55% 1,2-distearoyl-*sn*-glycero-3-phosphocholine (DSPC), 40% cholesterol and 5% DSPE-
116 PEG₂₀₀₀ (10 μ mol total lipid amount). The dried lipid film was hydrated 30 minutes at 65 °C (60
117 rpm) with 1 mL of a 120 mM ammonium sulfate salt solution. Extrusion was performed at
118 controlled temperature (65 °C) to ensure the fluidity of the lipids, using a homemade heating block
119 for the manual extruder. Finally, Doxil-Like liposomes were purified on a 1 x 20 cm Sephadex G-

120 50 (Medium) column equilibrated in a pH 7.4 buffer (5 mM Tris and 145 mM NaCl) to exchange
121 external medium. All liposome preparations (total final volume ~ 2 mL) were stored in darkness
122 at 4°C in 4 mL glass vials.

123 Liposome hydrodynamic diameter and ζ -potential were measured at 25°C using a Malvern
124 Zetasizer Nano ZS (Malvern, Worcestershire, UK) using the automatic algorithm mode at a
125 scattering angle of 173°. Size measurements, reported in intensity, were performed in a pH 7.4
126 buffer (5 mM Tris and 145 mM NaCl). ζ -potential measurements were obtained using the
127 Smoluchowski model by diluting the liposome sample in MiliQ purified water, using 0.1 mM total
128 lipid concentration in the cuvette. Experiments were run in triplicates or more.

129 2.4 Preparation of aptamer-loaded lipoplexes

130 Aptamer spiking solution (5% dextrose and 5 mM NaCl) was denatured 5 minutes at 95 °C,
131 vortexed for 1 minute and annealed at room temperature. Aptamer solution was then added
132 dropwise under stirring into 2.5 mM liposomal solution (1:1 v/v) at predefined N/P ratios (0.5 to
133 15). N is the number of amines (molar quantity of DOTAP) and P is the number of phosphorous
134 groups of aptamers (corresponding to the number of nucleotides). Lipoplexes were incubated in a
135 VorTemp 56 (Labnet, Edison, NJ) for 25 minutes, at 1000 rpm and 30 °C. Lipoplexes (total final
136 volume ~ 1 mL) were immediately used after incubation to determine the encapsulation efficiency
137 of aptamers. N/P ratio was optimized for each formulation to encapsulate more than 90% of
138 aptamers so that no further removal of unencapsulated aptamer was required.

139 2.5 Encapsulation efficiency of aptamers

140 Two methods were used to determine the encapsulation efficiency of aptamers into cationic
141 liposomes. Through the indirect method, the residual aptamer concentration in solution (1 to 150
142 nM) was quantified using fluorescent intercalating probes SYBRGold or SYBRGreen (Thermo

143 Scientific) for Apt-Ctrl-2 or all other aptamers, respectively. An aliquot of lipoplexes was diluted
144 to 300 μ L in 5% dextrose and 5 mM NaCl and centrifuged 60 minutes at 18500 g at room
145 temperature. The supernatant was diluted to fit in the linear range (1 to 150 nM) and SYBRGreen
146 100 X (or SYBRGold for Apt-Ctrl-2) was added (5% total volume). 150 μ L of each sample was
147 added to a 96-well plate and analyzed with a Safire microplate reader (Tecan, Männedorf,
148 Switzerland) (λ_{exc} 496 nm, λ_{em} 523 nm for both SYBRGreen and SYBRGold). A calibration curve
149 was determined for each DNA sequence. The amount of free DNA was determined and the
150 encapsulation efficiency was calculated using equation 1.

151 Equation 1: $EE (\%) = \frac{Total\ DNA - Free\ DNA}{Total\ DNA} * 100\%$

152 In addition, the amount of encapsulated aptamers within the lipoplexes was quantified directly
153 according to a second fluorescent assay. 2 mL of a solution of 1X SYBRGreen (or SYBRGold) in
154 5% dextrose and 5 mM NaCl was placed in a 3 mL cuvette. The fluorescence of this solution was
155 monitored over time on a F-2710 Spectrophotometer (Hitachi High Technologies America Inc.,
156 Schaumburg, IL, USA) at wavelengths of 496/523 nm ($\lambda_{exc}/\lambda_{em}$), under weak agitation. At t = 30
157 seconds, lipoplexes (corresponding to 100 nM DNA final concentration) were added in the cuvette,
158 and the accessible DNA increased the fluorescence of the SYBR probe. At t = 100 seconds, 10 μ L
159 of Triton X100 10% (v/v) was added to disrupt the liposomes, allowing the total amount of DNA
160 to be complexed by the SYBR probe. Final fluorescence was recorded at t = 200 seconds. The
161 percentage of aptamer encapsulation was calculated using the equation 2, where the initial intensity
162 is the average fluorescence intensity between time points 30 and 100 seconds and the final intensity
163 is the average fluorescence intensity between time points 100 and 200 seconds.

164 Equation 2: $EE (\%) = 100 - \left(\frac{Initial\ intensity}{Final\ intensity}\right) * 100\%$

165 2.6 Stability of lipoplexes

166 Lipoplexes, containing Doxapt-30 at N/P = 3, were prepared in 5% dextrose and 5 mM NaCl and
167 kept at 37 °C. Encapsulation efficiency of aptamers was measured by direct and indirect methods
168 at 0, 4 and 24 h to quantify the release of the Doxapt-30 aptamer. A similar study was conducted
169 on lipoplexes containing Apt-Ctrl-1 at N/P = 3. Encapsulation efficiency of aptamers was
170 measured at 0, 1, 2, 6, 8, 12 and 24 h in PBS at 37 °C. Colloidal stability studies were conducted
171 on another batch of lipoplexes containing Doxapt-30 at N/P = 3 diluted 3:1 in phosphate buffered
172 saline (PBS) at pH 7.4. The hydrodynamic diameter and polydispersity index were measured at
173 days 0, 3, 5 and 7.

174 2.7 Doxorubicin-loaded lipoplexes

175 Doxorubicin stock solutions were prepared in Tris/NaCl buffer (5 mM/145 mM, pH 7.4). Equal
176 volumes of lipoplexes and doxorubicin solutions were combined at various doxorubicin/aptamer
177 molar ratios (1:1 to 25:1). Noteworthy, Poly-Doxapt was composed of two pre-complexed strands
178 and considered as one molecule in the calculations (124 nucleic acid for one DNA molecule). The
179 mixture was incubated for 25 minutes, at 1000 rpm and 30 °C, and stored in the refrigerator in the
180 dark before use. Samples were used immediately to determine their encapsulation efficiency. N/P
181 ratio and drug/aptamer ratio were optimized for each formulation (Table 3). Optimized
182 formulations of doxorubicin-loaded lipoplexes were used without purification for *in vitro* release
183 and cytotoxicity studies, to ensure that doxorubicin total amount was identical in all samples.

184 As for Doxil-Like liposomes, doxorubicin stock solution was added to pH-gradient liposomes (1:1
185 v/v) to obtain drug/lipid ratio of 0.1 and the mixture was incubated at 50 °C, for 25 minutes and
186 1000 rpm. No further purification method was applied for subsequent testing.

187 Doxorubicin encapsulation was determined indirectly by fluorescence assay. Doxorubicin-loaded
188 lipoplexes were centrifuged 60 minutes at 18,500 g at room temperature and supernatant was

189 collected. Free doxorubicin was quantified by fluorescence using a Safire microplate reader (λ_{ex}
190 485 nm; λ_{em} 585 nm) against a calibration curve. Doxorubicin encapsulation efficiency was
191 determined using Eq 3. The final Drug/Lipid (D/L) ratio was determined using Eq 4.

192 Equation 3: $EE (\%) = \frac{(\text{Feeding doxorubicin}) - (\text{Free doxorubicin})}{(\text{Feeding doxorubicin})} * 100\%$

193 Equation 4: $D/L (w/w) = \frac{(\text{Feeding doxorubicin} - \text{Free doxorubicin})}{\text{Total lipid} + \text{Feeding doxorubicin}}$

194 2.8 Release kinetics of doxorubicin-loaded lipoplexes

195 Each formulation of doxorubicin-loaded lipoplexes was prepared in quadruplicate and used
196 without purification to ensure identical initial doxorubicin amounts in each condition. 1 mL of
197 doxorubicin-loaded lipoplexes (13 μM of doxorubicin) was added to dialysis bags (6-8 kDa
198 MWCO, Spectra/Por, Spectrum Laboratories, Inc) and immersed into 100 mL of PBS pH 7.4 (n
199 = 3) or acetate buffer pH 5 (n = 1). The whole set-up was moderately stirred at 37 °C and protected
200 from light. 0.8 mL samples were withdrawn from the external medium at predetermined time
201 points over 48 hours and replaced by fresh medium. Samples were stored at 4°C before analysis
202 with a UPLC-Fluorescence against a calibration curve prepared from the initial doxorubicin
203 solution. Briefly, the UPLC system (Shimadzu-Prominence UFLC, Shimadzu USA Manufacturing
204 inc. Mandel) consisted of a LC-20AD binary pump, a DGU-20A5 solvent degasser, a SIL-20AC
205 HT refrigerated, a CT0-20AC column oven and a RF-20AXS fluorescence detector. Mobile phase
206 A: water/0.1% formic acid. Mobile phase B: acetonitrile. Flow rate: 0.7 mL/min. Gradient A
207 decreased linearly from 90 to 60% between 0.25 to 5.5 min; followed by recovery of 90% A in 0.2
208 min, then equilibration for 4.5 minutes at 90% A. Total run time: 9 minutes. Injection volume: 50
209 μL . The column (Poroshell 120 EC-C18, 3.0 x 30 mm, 2.7 micron equipped with a pre-column
210 Agilent EC-C18, 3.0 x 5 mm, 2.7 micron) was kept at 30 °C and retention time of doxorubicin was
211 of 5.4 min. Detection of doxorubicin was measured at $\lambda_{\text{exc}} = 485 \text{ nm}$ / $\lambda_{\text{em}} = 585 \text{ nm}$. The kinetics

212 curves were also fitted using a double exponential function and the amplitude and rate constants
213 for drug release and drug degradation were obtained from the best fit.

214 2.9 Cell viability assay

215 HeLa cells were initially cultured in Eagle's Minimum Essential Medium (EMEM, ATCC® 30-
216 2003™) supplemented with 10 % fetal bovine serum (FBS) and 100 units/mL Penicillin-
217 streptomycin (Life Technologies, Burlington, ON). Cells were incubated at 37 °C with 5 % CO₂.
218 Cells were seeded in a 96-well plate at a density of 5 x 10³ cells per well. After 24 h, fresh culture
219 medium and optimized formulation were added to each well, with final concentrations of
220 doxorubicin ranging from 0.01 to 25 μM per well. In each plate, the blank formulation (without
221 doxorubicin) was tested for its cytotoxicity at its highest concentration used. After 48 h incubation,
222 the cells were rinsed with DPBS 1X. Resazurin in EMEM (final concentration of 44 μM in each
223 well) was added. The cells were incubated an additional 3 hours. Absorbance was measured at 570
224 nm and 600 nm to determine the metabolic reduction of resazurin. IC₅₀ was determined using
225 GraphPad Prism 6 and a normalized dose-response inhibition curve fitting. Each curve was made
226 in triplicate or more.

227 2.10 Tobramycin-loaded lipoplexes

228 Tobramycin sulphate was fluorescently labeled by Cy5. Synthesis details and characterization are
229 described in supplementary information. The binding affinity of Apt-Ctrl-1 for tobramycin-Cy5
230 was measured by fluorescence assay as described in supplementary information.

231 Before liposome preparation, Ctrl-Apt-1 was denatured 5 minutes at 95 °C, vortexed for 1 minute
232 and annealed at room temperature. Aptamer and Tobramycin-Cy5 were first mixed in equal
233 volumes at increasing molar ratios (0.5, 1, 2, 3, 5 tobramycin/aptamer) in 5% dextrose and 5 mM
234 NaCl. Liposomes (DOTAP/Chol/DSPE-PEG₂₀₀₀ 50/48/2 molar ratio) were previously prepared in

235 5% dextrose and 5 mM NaCl as described in section 2.3. They were mixed at equal volume (N/P
236 = 3) with the tobramycin/aptamer solutions or tobramycin solutions without Apt-Ctrl-1 (negative
237 control). The lipoplexes were incubated for 25 min at 30 °C at 1000 rpm before being centrifuged
238 60 minutes at 18,500 g at room temperature. Free tobramycin-Cy5 was quantified in the
239 supernatant by fluorescence using a Safire microplate reader (λ_{exc} 649 nm; λ_{em} 670 nm) against a
240 calibration curve. Tobramycin encapsulation efficiency and the final Drug/Lipid (D/L) ratio were
241 determined using Eq.3 and Eq.4 adapted to tobramycin. Experiment was run in triplicate.

242 2.11 Statistical analysis

243 Statistical analysis was carried out using PRISM 6.01 software (Graphpad, CA, USA). For zeta
244 potential measurements, statistical analysis was performed with two-tailed Student's t-test: *p <
245 0.05; **p < 0.01; ***p < 0.001. To determine statistically significant encapsulation efficiency
246 differences, a two-way ANOVA analysis was performed. To determine statistically significant
247 IC₅₀ differences, a one-way ANOVA analysis was performed. In both cases, P values for multiple
248 comparisons were adjusted using the Bonferroni correction. A P value of ≤ 0.05 was considered
249 significant.

250

251 **Results**

252 3.1 Aptamer design and affinity for doxorubicin

253 In this study, we used aptamers as the driving force to actively load a drug into the liposomes.
254 Doxorubicin was selected as a model drug for several reasons. First, it represents a good example
255 of successful active drug loading via ammonium sulphate gradient into liposomes [22]. Second, a
256 doxorubicin-binding DNA aptamer has already been reported and validated in the literature [33,

257 36]. Third, binding of doxorubicin to aptamers can be easily monitored by fluorescence
258 measurements, which makes it a suitable model drug candidate for formulation optimization [37].
259 We hypothesized that tuning the affinity of the aptamers should impact the loading and the release
260 rate of the drug from liposomes, therefore we designed a series of aptamer sequences with various
261 binding properties, (Figure 1A, Table S1). All the aptamers include the doxorubicin specific
262 sequence, designed as Doxapt-28 [36]. Doxapt-30 possesses an extra base pair that should stabilize
263 the double strand section and increase the affinity of the aptamer for its ligand [33]. Coop-Doxapt,
264 a two-binding-site aptamer reported by Simon *et al.*, contains two binding sites and displays a
265 cooperative binding behaviour [33]. Inspired by polymer-like aptamers [38], we also created Poly-
266 Doxapt to improve aptamer packing into the liposome. Finally, two sequences were used as
267 negative controls: Apta-Ctrl-1 is a 21-nucleotide aptamer designed for tobramycin, which presents
268 a hairpin structure, but no specificity for doxorubicin [39] and Apta-Ctrl-2 is a 30mer of poly-
269 thymine without any secondary structure. Following the proof-of-concept demonstration, the
270 strategy was applied to another drug, tobramycin, using the reported specific aptamer sequence
271 Apt-Ctrl-1 (Figure 1A) [39].

272 Once intercalated into a DNA, doxorubicin fluorescence is quenched, which allows monitoring of
273 its interaction with different aptamer structures (Figure 1B) [37]. Dissociation constants (K_D) of
274 the various aptamers in the medium used for liposomal formulation (dextrose 5%, 5 mM NaCl)
275 can thus be obtained by fitting the fluorescence intensity of doxorubicin to increasing
276 concentrations of aptamers. A representative example of such curves is displayed in Figure 1C
277 (see also Figures S1-S5) and the summary of all K_D is provided in Table 1. Doxapt-28 (380 nM)
278 and Doxapt-30 (334 nM) exhibit K_D values in agreement with previous reports, despite variation
279 of the medium (Table 1) [33]. Both Coop-Doxapt and Poly-Doxapt exhibited a higher affinity for

280 doxorubicin (160 ± 36 nM and 68 ± 6 nM respectively), confirming the relevance of multivalent
281 aptamers. However, under the liposomal formulation conditions, however, Coop-Doxapt did not
282 display a higher cooperativity for doxorubicin binding as this has been previously observed at
283 higher temperature (30°C) and ionic strength (50 mM) (Figure S3) [33]. This is likely due to the
284 fact that the cooperativity level of DNA recognition elements are highly dependent on temperature
285 and ionic strength variations [40]. Finally, Apt-Ctrl-1 displayed reduced affinity for doxorubicin
286 ($K_D > 1000$ nM) while Apt-Ctrl-2 did not quench the fluorescence at an appreciable amount to
287 determine a dissociation constant. Overall, this collection of aptamers exhibits dissociation
288 constants for doxorubicin ranging from 68 nM to > 1000 nM.

289 3.2 Lipoplex preparation and characterization

290 Aptamers were incorporated into cationic liposomes via electrostatic interactions. The liposome
291 composition (DOTAP/Chol/DSPE-PEG₂₀₀₀ 50/48/2) was inspired by the widely reported lipid
292 formulations used in gene delivery [41]. Similarly to these latter systems, the physico-chemical
293 properties of lipoplexes rely on the charge ratio N/P (amino group of DOTAP vs. phosphate group
294 of nucleotide). As illustrated by Doxapt-30 lipoplexes, the liposome increased in size upon
295 incubation with aptamers and exhibited aggregation at the charge ratio N/P = 2, as witnessed by
296 the higher diameter and polydispersity index (Figure 2A). Colloidal stability is recovered with an
297 excess of cationic charges (N/P ≥ 3), resulting in lipoplexes smaller than 200 nm diameter, with
298 low polydispersity and positive ζ potential (Figure 2A&B). Similar behaviour was confirmed for
299 all aptamers (Figure S6). Aptamer complexation efficiency, quantified by the remaining DNA in
300 solution, was also improved with increasing charge ratios. Aptamers presenting one binding site
301 (Doxapt-28 and Doxapt-30) required N/P = 3 to be fully encapsulated into liposomes, whereas N/P

302 = 2 was sufficient for Coop-Doxapt and Poly-Doxapt to achieve complete DNA complexation
303 (Figure 2C). These results were confirmed by directly measuring the concentration of aptamers
304 within lipoplexes (Table S2). Except for Coop-Doxapt and Poly-Doxapt, the values obtained (\geq
305 94% for all aptamers) demonstrated that DNA was mainly encapsulated within lipoplexes; only a
306 minor quantity was adsorbed on the surface. Noteworthy, ζ potential of Poly-Doxapt and Coop-
307 Doxapt were still negative at N/P = 2, suggesting the presence of DNA strains adsorbed on the
308 surface of the lipoplexes (Table 3). This could be due to the longer sequence of nucleotides of
309 Coop-Doxapt and Poly-Doxapt (86 and 124 nucleotides, respectively) as compared to other
310 aptamers (28-30 nucleotides). Adsorption of Coop-Doxapt was confirmed since only 46% of the
311 aptamer was actually encapsulated within the lipoplex structure, as determined by direct
312 measurement (Table S2). As for Poly-Doxapt, direct and indirect methods corroborate that more
313 than 83% of aptamers were encapsulated within liposomes (Table S2). This result suggests that,
314 despite the negative zeta potential, aptamers were tightly bound to the lipoplex structure and were
315 not accessible to the fluorescent dye.

316 In addition, the aptamers remained encapsulated for at least 24h at 37°C, for Doxapt-30 (Table 2)
317 as well as for the control sequence Apt-Ctrl-1 (Table S3). For each aptamer, optimal N/P ratio was
318 selected as the lowest ratio leading to stable lipoplexes and maximal encapsulation of aptamer
319 (Table 3). Final lipoplexes exhibited diameters ranging from 170 to 290 nm with low
320 polydispersity indexes, and almost complete complexation of aptamers. Lipoplexes exhibited good
321 colloidal stability for 7 days in PBS at 37°C (Figure S7).

322 3.3 Encapsulation of doxorubicin

323 Aptamer-loaded lipoplexes were further incubated with doxorubicin at increasing
324 doxorubicin/aptamer molar ratios, and doxorubicin encapsulation was quantified by fluorescence
325 of free drug after centrifugation. A representative behaviour is reported on Figure 3A with Doxapt-
326 30. Encapsulation efficiency (EE) reached $\geq 85\%$ doxorubicin for up to 2 drug molecules per
327 aptamer, close to the efficiency of the sulphate gradient method of Doxil-Like liposomes (Figure
328 3A). The active role of aptamers in the loading capacity was confirmed by a series of controls.
329 Passive encapsulation was estimated to range from 5 to 25% using cationic or plain liposomes,
330 respectively (Figure 3A). Moreover, Apt-Ctrl-2 (Poly-thymine) was not able to drag doxorubicin
331 into the liposomes whereas Apt-Ctrl-1, presenting a hairpin structure, displayed 45% reduction
332 compared to the highest doxorubicin encapsulation value, which confirmed the higher specificity
333 of Doxapt-30 for doxorubicin. Interestingly, the lipoplexes of Doxapt-30 enabled the loading of
334 more than 2 doxorubicin molecules per aptamer, although this sequence is designed to have only
335 one binding site. Above this doxorubicin/aptamer ratio, additional drug loading was reduced,
336 leading to a decrease of EE %. Nonetheless, the final drug/lipid ratio (D/L) still increased up to 20
337 doxorubicin/aptamer (Figure 3A). Similar trends were also observed for Coop-Doxapt and Poly-
338 Doxapt, which were found to load up to 8 and 15 equivalents of doxorubicin with more than 80%
339 EE for Coop-Doxapt and Poly-Doxapt, respectively (Figure 3B). Therefore, the adsorption of
340 Coop-Doxapt on the surface of lipoplexes did not seem to impact its loading capacity. In contrast,
341 Doxapt-28 loaded lipoplexes were not able to encapsulate more than 45 % doxorubicin. This could
342 be due to the deletion of one base pair in the Doxapt-28 sequence (Figure 1A), which leads to a
343 less stable stem-loop (1 GC less, around 2 kCal/mol) [42]. The Doxapt-28 stem-loop may be
344 destabilized in the lipoplex structure, which may impair doxorubicin binding. Therefore, Doxapt-
345 28 appears as a negative control of Doxapt-30, exhibiting the closest sequence as possible with

346 significantly different loading properties. A summary of the optimized formulations is presented
347 on Table 3. For each aptamer, we selected the formulation exhibiting high encapsulation of both
348 aptamer and doxorubicin, with a minimum amount of excipients. Furthermore, the addition of
349 doxorubicin to lipoplexes did not significantly affect neither the size nor the polydispersity of the
350 formulations (Table 3). Further studies were conducted using twice the doxorubicin amount as
351 compared to the number of binding sites, to maximize drug loading for both single and double-
352 binding sites aptamers.

353 3.4 Release kinetics of doxorubicin-loaded lipoplexes

354 Aptamers improve the loading capacity of liposomes but do their presence impact drug release
355 rate? To test this question, we measured the release kinetics of doxorubicin from the aptamer-
356 loaded lipoplexes by employing a dialysis method (Figure 4). Lipoplexes were prepared at optimal
357 ratios and were not purified before dialysis, to ensure similar initial doxorubicin concentration.
358 Kinetics display a bi-exponential profile with the fastest transition representing the release of
359 doxorubicin from the lipoplexes and the slowest transition the elimination of doxorubicin over
360 time (Table 4 and Figure S8). The elimination of doxorubicin concentration after several hours
361 (Figure 4) might be due to the degradation of doxorubicin at pH 7.4 at 37°C and its adsorption to
362 surfaces (dialysis bags as well as sampling vials), as previously described [43, 44]. In agreement
363 with literature, Doxil-Like liposomes exhibited a lower release efficiency (less than 15% after 48
364 hours, Figure 4) [22, 45] but the observed release rate was found similar to the rate obtained for
365 free doxorubicin control (Table 4). This could be due to some doxorubicin adsorbed on the
366 liposome surface, which was washed out in the first hour. Interestingly, quite different profiles
367 were obtained for the series of lipoplexes. The high-loading Coop-Doxapt lipoplexes, for example,

368 released 5-fold more doxorubicin than the Doxil-like liposomes at a 5-fold slower rate (0.20 ± 0.05
369 hr^{-1}) reaching 80% of drug release after 10 hours (Figure 4). This suggests that doxorubicin release
370 was slowed down by the binding to the aptamer but the adsorption of Coop-Doxapt on the lipoplex
371 surface favored doxorubicin extensive release. Poly-Doxapt, which possesses the highest affinity
372 for doxorubicin, released doxorubicin 5-fold slower than the Coop-Doxapt ($0.04 \pm 0.01 \text{ h}^{-1}$), which
373 resulted in only 20% of doxorubicin being released after 48 h, similar to the Doxil-Like
374 formulation (Figure 4). Doxapt-30, which has an intermediate affinity ($K_D = 334 \text{ nM}$), displayed a
375 sustained release, achieving 30% of release after 12 hours with a release rate similar to Coop-
376 Doxapt ($0.23 \pm 0.06 \text{ h}^{-1}$). Doxapt-28 also displayed a similar release rate (Table 4), despite its low
377 drug loading efficiency, while Apta-Ctrl 1 displayed a significantly faster release rate of $0.38 \pm$
378 0.07 h^{-1} , in agreement with its lower affinity for doxorubicin. Both latter formulations released
379 more doxorubicin than Doxapt-30 (75% and 45% of initial doxorubicin after 12 hours,
380 respectively), probably due to the residual unencapsulated doxorubicin. As a control, we
381 demonstrated that no leakage of Doxapt-30 nor the Apta-Ctrl-1 was detected over a 24h period in
382 the same conditions, showing no sequence specific effect on aptamer release (Table 2 & Table
383 S3). We also investigated the behaviour of doxorubicin loaded lipoplexes at acidic pH, to mimic
384 the endosomal conditions. Interestingly, the relative behaviour of aptamers was maintained albeit
385 the acidic conditions decreased doxorubicin elimination, in agreement with literature [44], which
386 slightly increased the extent of drug release (Figure S9 and S10). Coop-Doxapt and Doxapt-30
387 still exhibited similar release rates (0.30 and 0.28 h^{-1} , respectively, Table 4). Here again, Coop-
388 Doxapt released over 90% of its drug in 12 hours (Figure S9) whereas Doxapt-30 sustained its
389 release (53% doxorubicin released in 12 hours). The higher affinity of Poly-Doxapt severely
390 reduced doxorubicin release (22% in 12 hours, Figure S9) as well as the release rate (0.078 h^{-1} ,

391 Table 4). The negative controls, Doxapt-28 and Apta-Ctrl-1, still quickly released 82 and 72% of
392 their content after 12 hours, respectively (Figure S9). Overall, these results suggest that aptamers
393 slowed down the release of drug according to their specific affinity, which allows to control drug
394 diffusion and release from lipoplexes.

395 3.5 Cell viability assay

396 Modifying the release kinetics of a drug has a direct impact on its therapeutic efficacy. To explore
397 this impact, we completed our study by assessing the cytotoxic activity of doxorubicin in the
398 optimized formulations on HeLa cells (Figure 5A). Free doxorubicin presented an IC_{50} of $1.5 \pm$
399 $0.6 \mu\text{M}$, in agreement with the literature [46]. Doxil-Like formulation exhibited significantly
400 higher values of IC_{50} , up to $38 \mu\text{M}$, reflecting of the low immediate bioavailability of doxorubicin
401 from these liposomes. Doxapt-30 improved 4 times the therapeutic efficacy of Doxil-Like
402 formulation, exhibiting similar cytotoxicity as free doxorubicin, notwithstanding its sustained
403 release. Coop-Doxapt and Apta-Ctrl 1 also exhibited similar cytotoxicity to free doxorubicin,
404 probably due to their extensive drug release over 48 hours. Conversely, Poly-Doxapt exhibited
405 similar cytotoxicity to Doxil-Like formulations, in agreement with its low doxorubicin release, in
406 addition to its negative zeta potential and low N/P ratio, which may reduce cellular uptake [47].
407 As a control of lipoplex influence, the cell viability was determined after incubation with the
408 highest concentration of aptamer-loaded lipoplexes without doxorubicin (Figure 5B). The four
409 blank lipoplexes formulations exhibited no toxicity on HeLa cells at their highest concentration,
410 and were better tolerated than Doxil-Like formulation. Overall, these results demonstrate that
411 aptamer binding to doxorubicin did not prevent therapeutic efficacy of the drug, and an adequate

412 sequence design could even improve its availability as compared to ammonium sulphate gradient
413 liposomes.

414 3.6 Application to tobramycin

415 Encouraged by this proof-of-concept, we further applied the strategy of aptamer-loaded lipoplexes
416 to another drug, tobramycin. In the treatment of lung infection, liposomal tobramycin
417 demonstrated drug retention in the lung and improved *in vivo* efficacy against bacterial infection
418 as compared to the free drug [48]. Liposomes have also allowed a better accumulation close to the
419 bacterial biofilm but the antibiotic activity was limited due to the low encapsulation efficiency of
420 liposomes [49]. Indeed, tobramycin aminoglycoside structure is highly hydrophilic, which
421 prevents its efficient encapsulation within liposomes. Therefore, this drug would significantly
422 benefit from an active loading strategy using drug specific aptamers. Apt-Ctrl-1 was selected for
423 its reported affinity for tobramycin [39]. To facilitate detection, tobramycin sulphate was labeled
424 by fluorescent Cy5 (see synthesis and characterization in supporting information). Binding affinity
425 of Apt-Ctrl-1 for tobramycin was determined to be $1.15 \pm 0.24 \mu\text{M}$, slightly higher than
426 doxorubicin-binding aptamers (Figure 6A). Encapsulation of tobramycin in cationic liposomes
427 was compared with or without aptamers (Figure 6B). Interestingly, aptamers do also improve the
428 encapsulation of tobramycin, reaching 5.8 times greater EE at high concentrations of tobramycin
429 (45% against 8%, with and without aptamer, respectively) as well as drug/lipid ratio. These results
430 demonstrate that an aptamer-loading strategy could successfully be used to improve the loading
431 efficiency of various drugs into liposomes, especially for drugs with low encapsulation properties.

432 **Discussion**

433 Loading of drugs into liposomes is a critical step of the liposomal formulation, since it determines
434 the amount of excipient required, as well as the factors governing the release rate of the drug [21].
435 In the passive loading method, the drug dissolved in the aqueous phase equilibrates with the
436 liposome's internal medium, which limits its encapsulation efficiency. Higher scores can be
437 achieved using a gradient method, such as pH or ions (ammonium sulphate, hydrogenophosphate,
438 or metallic ion such as copper or manganese salts) [19]. In this strategy, the drug, when present
439 inside the vesicle core, is converted to an ionic/salt form, which is unable to diffuse back through
440 the lipid membrane, thus is retained into the liposome core. Unfortunately, this strategy also
441 strongly impairs the release rate of the drug, and often requires an additional trigger [24]. This is
442 confirmed by our results of Doxil-Like formulation, which exhibited limited release (Figure 4),
443 high IC_{50} on HeLa cells, and even a non-negligible toxicity of the liposomes itself (Figure 5).

444 We prepared liposomes with drug-specific aptamers to improve the loading capacity of liposomes.
445 We selected aptamer technology because (i) their affinity can be tuned by controlling their
446 nucleotide sequence or length [42], allowing to optimize the aptamer sequence according to the
447 desired release properties; (ii) the binding does not change the protonation of the drug, therefore
448 maintaining its diffusion and release ability [34] and (iii) aptamers could be designed for almost
449 any target, suggesting this strategy could be applied to a large range of molecules [3].

450 The series of aptamers was designed to study the relationship between the sequence and the
451 properties of aptamer-loaded lipoplexes. As expected, the affinity of aptamers varied according to
452 their sequences and binding sites (Table 1). The results confirmed the specificity of the aptamer
453 sequences for its drug since the binding is higher than the natural affinity of doxorubicin for
454 random single or double-stranded DNA (Table 1) as well as aptamer/doxorubicin complexes

455 reported in literature ($K_D \approx 600$ nM) [37]. However, Doxapt-28, presenting a similar affinity to
456 Doxapt-30, was not able to encapsulate more than 50% of doxorubicin. Adding a base pair to the
457 hairpin probably allowed a higher stabilization of the complex, which has already been reported
458 [42]. The three other structures, although exhibiting different binding constants, demonstrated
459 similar drug loading capacity (Table 3). This might be explained by the high concentration of the
460 drug in the liposomal formulation (more than 10 times K_D) resulting in the saturation of aptamers.
461 These conditions might also reveal secondary binding sites on aptamers, which results in the
462 binding of more than 2 doxorubicin molecules per aptamer for Doxapt-30 and more than 8 and 15
463 molecules for Coop-Doxapt and Poly-Doxapt, respectively (Figure 3). For the latter cases, the
464 higher loading capacity may be linked to their longer sequence of nucleotides (86 and 124
465 nucleotides, respectively), revealing probably additional binding sites for doxorubicin.
466 Interestingly, this behaviour was also observed for tobramycin (Figure 6B), which was able to
467 encapsulate up to 2.5 tobramycin equivalents, although designed with only one binding site.
468 Although this non-specific binding was not detected in the binding affinity measurements (Figure
469 1), it can be explained by the natural affinity of doxorubicin for nucleic acids or the electrostatic
470 interactions of both cationic drugs with anionic nucleobases [37, 50]. In addition, incorporation of
471 DNA sequences into liposomes has been reported to strongly impact the structural organization of
472 the liposome, resulting in densely packed lipoplexes, which might favor the retention of the drug
473 [50, 51]. Overall, aptamer incorporation into liposomes significantly improved their loading
474 capacity, through specific as well as non-specific interactions with the drug.

475 Interestingly, our results show that release kinetics and therapeutic efficacy could be tuned
476 according to the aptamer structure. We showed that drug binding to the aptamer slowed down the
477 release rate of the drug in comparison to the free drug, according to its affinity constant. Doxapt-

478 30 exhibited a slower release than Apt-Ctrl-1, which allowed a sustained release of the drug over
479 48 hours. Nevertheless, a too high affinity might compromise the drug release from the lipoplex,
480 as exemplified by Poly-Doxapt ($K_D = 68$ nM, less than 15% release in 48 hours). Therefore, this
481 latter system did not improve commercial formulation, as confirmed by the same therapeutic
482 efficiency as Doxil-Like (Figure 5). Apart from the affinity, our results suggest that other sequence
483 parameters impact the overall behaviour of the system. Coop-Doxapt, maybe due to its longer
484 stem-loop, resulted in low encapsulation of aptamer within the lipoplex. The adsorption of ~ 50%
485 Coop-Doxapt on the surface of liposomes still allowed doxorubicin complexation but favored its
486 release in physiological conditions. Therefore, this system was not improved compared to free
487 doxorubicin. In the other hand, the short Doxapt-28 sequence demonstrated that a minimal stability
488 of the stem-loop is required to ensure drug binding ability within the lipoplex structure. In our
489 study, Doxapt-30 exhibited the advantages of Doxil-Like formulation without its limitations.
490 Indeed, this sequence exhibits a specific affinity for doxorubicin and a high encapsulation
491 efficiency within cationic lipoplexes, which resulted in a sustained release profile and an excellent
492 therapeutic efficiency. In addition, this nucleotide sequence length limited the excipient mass
493 required for doxorubicin loading, resulting in the highest drug/lipid ratio (Table 3).

494 **Conclusion**

495 In conclusion, we developed a new strategy of drug loading, by designing drug-specific aptamers
496 to drive drugs into liposomes. Combining the advantages of aptamer specific properties and
497 liposomal controlled release enable to achieve tunable properties according to the structure of the
498 aptamer. We demonstrated the proof-of-concept using doxorubicin, but this strategy may be
499 applied to a large variety of drugs, since aptamers can be synthetically prepared against about any

500 target, from small molecules to whole cells. In particular, we showed that aptamers significantly
501 improved the loading of hydrophilic tobramycin into liposomes. These results demonstrate the
502 potential of aptamer technology for multifunctional drug delivery systems. In particular, adding
503 drug specific sequences to a cancer-targeted aptamer could lead to better controlled drug delivery
504 systems. Further improvements are currently focused on the drug/lipid ratio and the application to
505 larger biomacromolecules.

506 **Acknowledgements**

507 Financial support from Réseau Québécois de Recherche sur le Médicament (RQRM), Hydro-
508 Quebec and University of Montreal is acknowledged for the scholarship of K. Plourde. The authors
509 want to thank Alexandre Melkoumov for synthesizing Tobramycin-Cy5 and performing statistical
510 analysis, Warren Viricel for his help in graphics, Mihaela Friciu for her help in HPLC analysis and
511 Jennifer Jean-Louis for the stability study. J. Leblond Chain thanks Pr N. Bertrand for insightful
512 discussions.

513

514 Table 1. Characteristics of aptamers used in this study and their affinity constants (K_D) for
 515 doxorubicin.

Formulation	Doxapt-28	Doxapt-30	Coop-Doxapt	Poly-Doxapt	Apt-Ctrl-1	Apt-Ctrl-2
Nucleotides	28	30	86	62 +62	21	30
Binding sites	1	1	2	2	0	0
K_D (nM) ¹	380 ± 45	334 ± 29	160 ± 36	68 ± 6	> 1000	ND ²

516 ¹ *Determined by fluorescence assay, as shown in Fig 1, S1-S5.*

517 ² *Fluorescence of doxorubicin was not quenched sufficiently to determine a dissociation constant (see Figure S5).*

518

519 Table 2. Stability of encapsulated aptamers over 24 h at 37 °C in dextrose 5% NaCl 5 mM.

520 Liposomes DOTAP/Chol/DSPE-PEG₂₀₀₀ 50/48/2 encapsulating Doxapt-30 (ratio N/P = 3) were

521 assayed for their content in aptamers using the direct and indirect method. Results are reported as

522 the mean value of 3 experiments, ± standard deviation of the mean.

Time (h)	0	4	24
Direct method	98.3 ± 0.1 %	98.1 ± 0.1 %	98.2 ± 0.1%
Indirect method	98.6 ± 0.6 %	99.1 ± 0.3 %	97.0 ± 1.2 %

523

524

525

526

527 Table 3: Summary of the characteristics for the optimized formulations of liposomes, lipoplexes containing aptamers and doxorubicin-
 528 loaded lipoplexes. All liposomes were cationic liposomes (DOTAP/Chol/DSPE-PEG₂₀₀₀ 50/48/2 molar ratio) except for Doxil-Like
 529 (DSPC/Cholesterol/DSPE-PEG₂₀₀₀ 55/40/5 molar ratio). Results are reported as the mean value of 3 measurements, \pm standard deviation
 530 of the mean.

Formulation		Doxapt-28	Doxapt-30	Coop-Doxapt	Poly-Doxapt	No Apta	Doxil-Like	Apt-Ctrl-1	Apt-Ctrl-2
Liposomes	Z-Average Diameter (nm)	139 \pm 3	154 \pm 2	139 \pm 3	139 \pm 3	139 \pm 3	187 \pm 6	139 \pm 3	139 \pm 3
	PdI	0.082 \pm 0.001	0.049 \pm 0.012	0.082 \pm 0.001	0.082 \pm 0.001	0.082 \pm 0.001	0.038 \pm 0.036	0.082 \pm 0.001	0.082 \pm 0.001
Aptamer-loaded Lipoplexes	Z-Average Diameter (nm)	171 \pm 3	286 \pm 2	230 \pm 3	283 \pm 7	139 \pm 3	187 \pm 6	242 \pm 5	206 \pm 4
	PdI	0.058 \pm 0.018	0.241 \pm 0.018	0.058 \pm 0.019	0.222 \pm 0.023	0.082 \pm 0.001	0.038 \pm 0.036	0.069 \pm 0.013	0.048 \pm 0.033
	Zeta potential (mV)	22.4 \pm 1.2	28.2 \pm 0.6	-19.4 \pm 0.6	-24.7 \pm 0.6	24.9 \pm 0.6	-4.8 \pm 1.1	4.53 \pm 0.6	17.6 \pm 1.6
	Ratio N/P	3	3	2	2	N/A	N/A	3	3
	EE% Aptamers ^a	94 \pm 2%	100 \pm 0%	99 \pm 2%	98 \pm 1%	N/A	N/A	94 \pm 1%	99 \pm 0%
Doxorubicin and aptamer-loaded lipoplexes	Z-Average Diameter (nm)	197 \pm 2	236 \pm 6	254 \pm 2	312 \pm 4	154 \pm 2	181 \pm 3	285 \pm 5	204 \pm 2
	PdI	0.058 \pm 0.018	0.047 \pm 0.048	0.062 \pm 0.002	0.172 \pm 0.007	0.074 \pm 0.008	0.063 \pm 0.010	0.075 \pm 0.011	0.068 \pm 0.029
	Zeta potential (mV)	16.3 \pm 0.8	15.9 \pm 0.7	-28.1 \pm 1.7	-28.8 \pm 1.2	20.9 \pm 0.9	-11.5 \pm 0.1	8.81 \pm 0.7	5.7 \pm 0.5
	Ratio Dox/Apta	2	2	4	4	N/A	N/A	2	2
	EE% Dox ^b	28 \pm 7%	84 \pm 2%	73 \pm 3%	86 \pm 1%	5 \pm 3%	98 \pm 1%	39 \pm 0%	7 \pm 5%
	Final D/L ratio ^c	0.0034	0.0092	0.0088	0.0069	0.0006	0.098	0.0062	0.0008

531 ^a Determined by indirect method using Eq 1.

532 ^b Determined by indirect method using Eq 3.

533 ^c D/L: Drug / Lipid ratio (w/w) determined using Eq 4.

534

535

536
 537 Table 4. Kinetic parameters of doxorubicin release from the aptamer-loaded lipoplexes at pH 7.4 (see Figure 4) and pH 5 (See Figure
 538 S9). All kinetics were fitted using a bi-exponential fit. The fastest transition (described by Amplitude 1 and Rate 1) represents the
 539 release of doxorubicin from the lipoplexes and the slowest transition (described by Amplitude 2 and Rate 2) the degradation of
 540 doxorubicin over time. No degradation was evidenced at pH 5.
 541
 542
 543

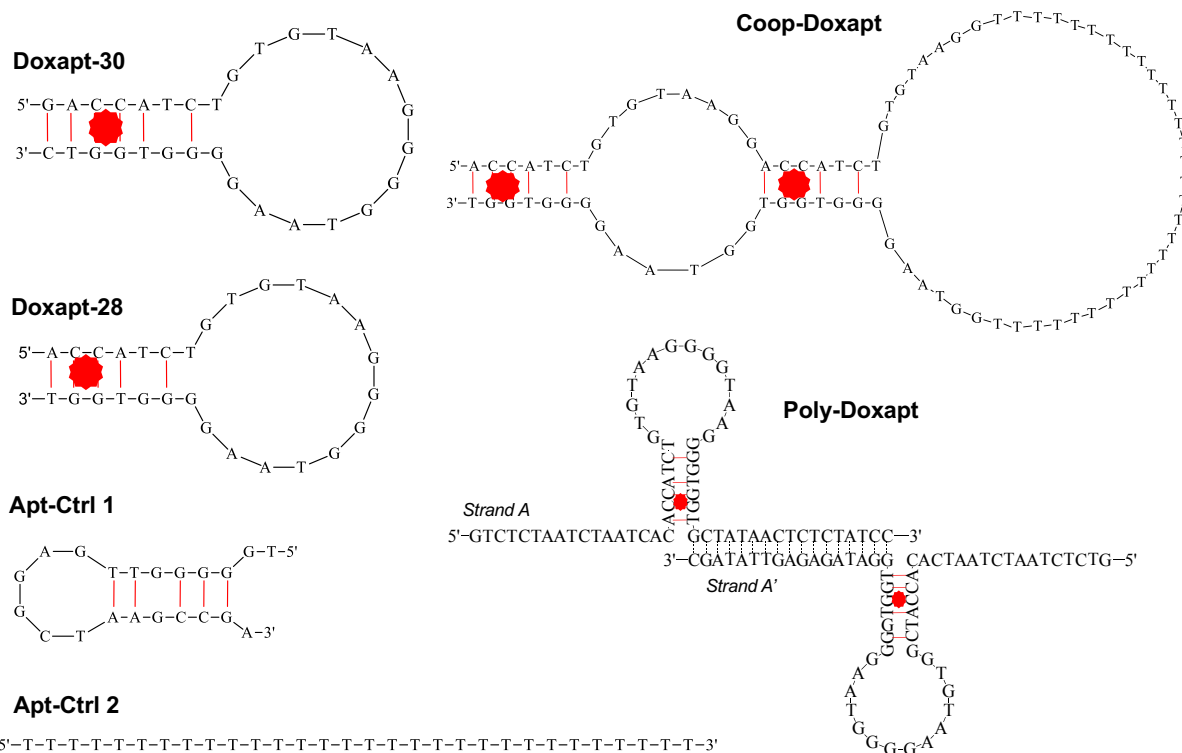
		Free Dox	Doxil-Like	Coop-Doxapt	Poly-Doxapt	Doxapt-30	Doxapt-28	Apta-Ctr-1
pH 7.4	Amp 1 ¹	-102 ± 8	-16 ± 2	-136 ± 23	-21 ± 4	-52 ± 9	-130 ± 20	48 ± 2
	Rate 1 ²	0.8 ± 0.1	1.2 ± 0.3	0.20 ± 0.05	0.04 ± 0.01	0.23 ± 0.06	0.20 ± 0.04	0.38 ± 0.07
	Amp 2 ¹	99 ± 8	16 ± 1	128 ± 25	-	49 ± 10	123 ± 21	-
	Rate 2 ²	0.039±0.006	0.016±0.005	0.025±0.007	-	0.028±0.007	0.027±0.007	-
pH 5	Amp 1 ¹	-	-	-93 ± 2	-34 ± 1	-55 ± 2	-80 ± 5	73 ± 3
	Rate 1 ²	-	-	0.30 ± 0.01	0.078 ± 0.007	0.28 ± 0.03	0.52 ± 0.07	0.30 ± 0.06

553
 554 ¹ In %

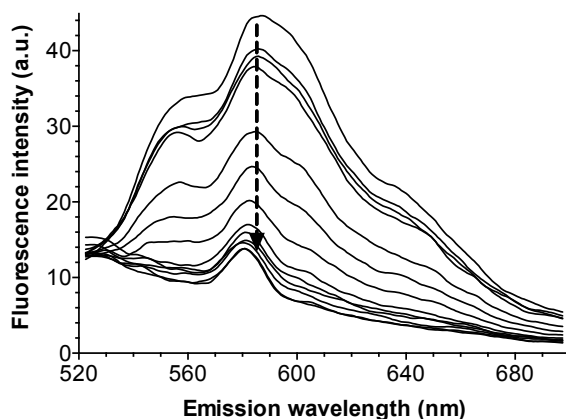
555 ² h⁻¹

556

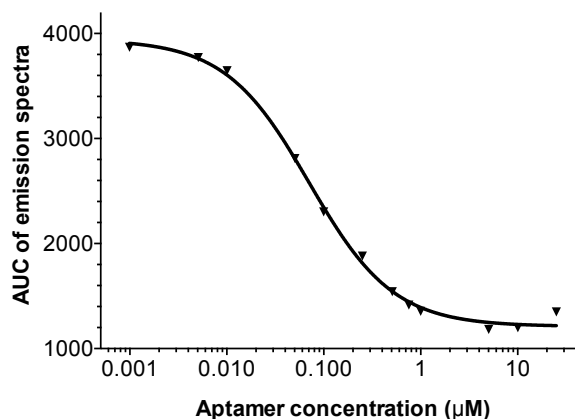
A



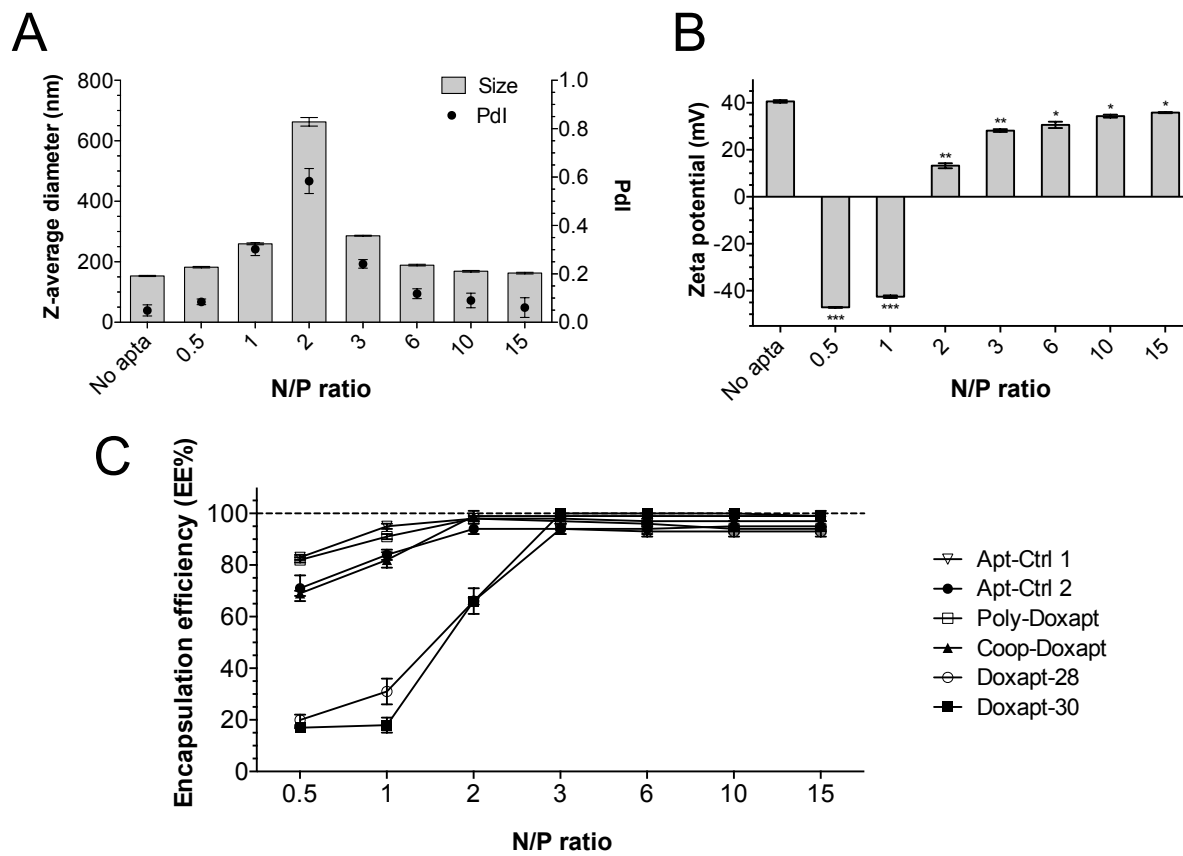
B



C



557
 558 Figure 1. Design of doxorubicin-binding aptamers with various affinities. A) Structure of DNA
 559 sequences designed for doxorubicin. The binding site for doxorubicin is suggested by a dot. B)
 560 Smoothed emission spectra of doxorubicin (100 nM in 5% dextrose and 5 mM NaCl) with
 561 increasing concentration of Poly-Doxapt (from top to bottom, 0, 0.001, 0.005, 0.01, 0.05, 0.1, 0.25,
 562 0.75, 1, 5, 10, 25 μM). C) Representative determination of affinity binding constant K_D for Poly-
 563 Doxapt. Each point represents the area under the curve of the fluorescence emission spectra
 564 showed in B).
 565

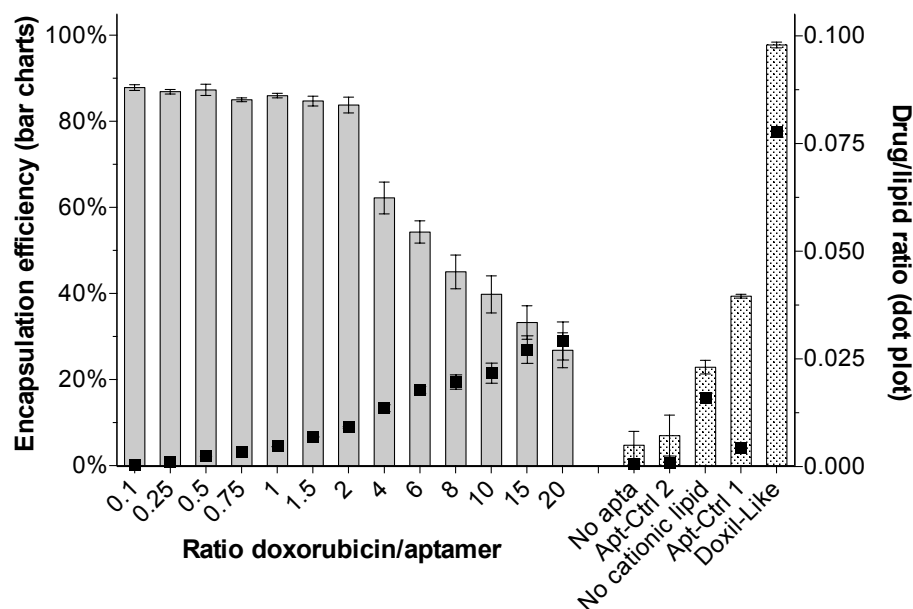


566

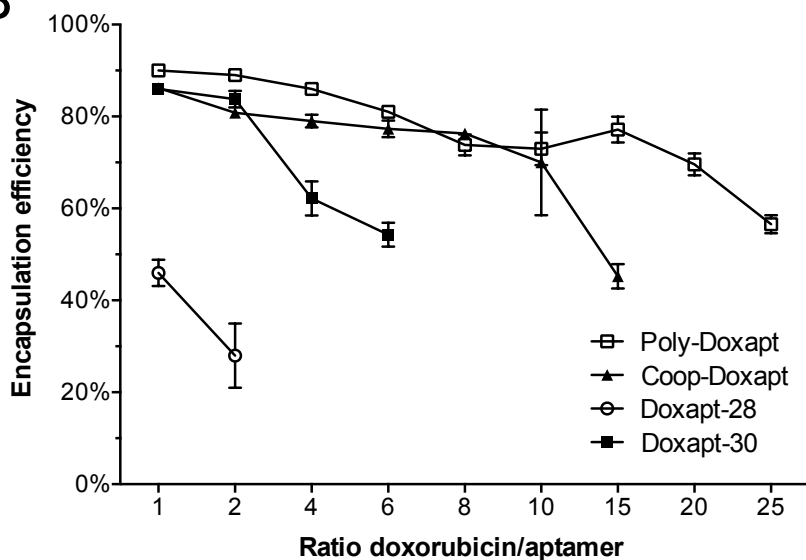
567 Figure 2. Optimization of aptamer-loaded liposomes (DOTAP/Chol/DSPE-PEG₂₀₀₀ 50/48/2 molar
 568 ratio) according to the N/P ratio (amine of DOTAP/phosphate of nucleobases). A) Hydrodynamic
 569 diameter (Size) and polydispersity index (PdI) and B) Zeta potential measurements of lipoplexes
 570 encapsulating Doxapt-30. Statistical analysis performed with two-tailed Student's t-test: *p < 0.05;
 571 **p < 0.01; ***p < 0.001. C) Encapsulation efficiency of all aptamers within cationic lipoplexes.
 572 Results are reported as the mean value of 3 measurements, ± standard deviation of the mean.

573

A



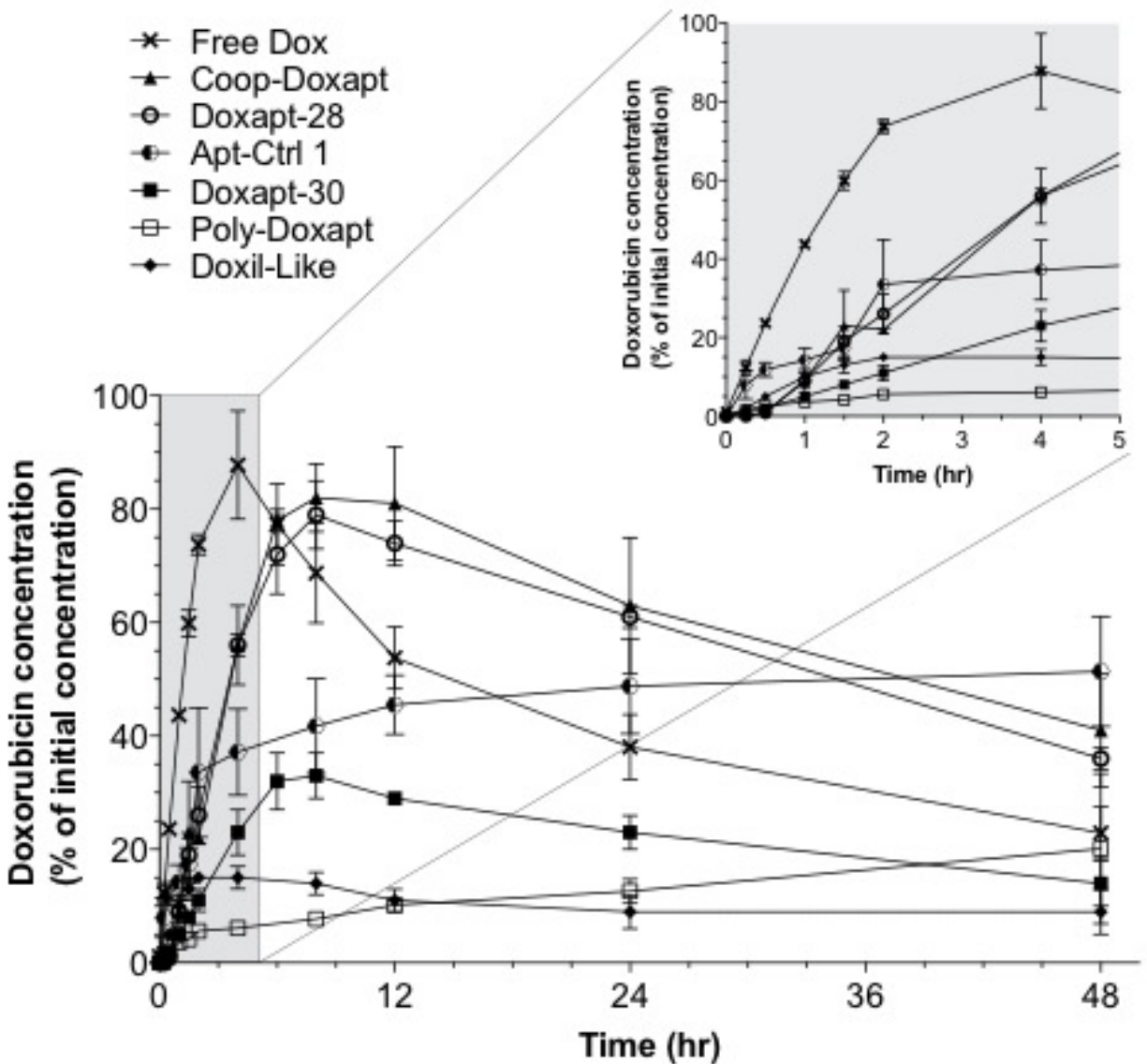
B



574

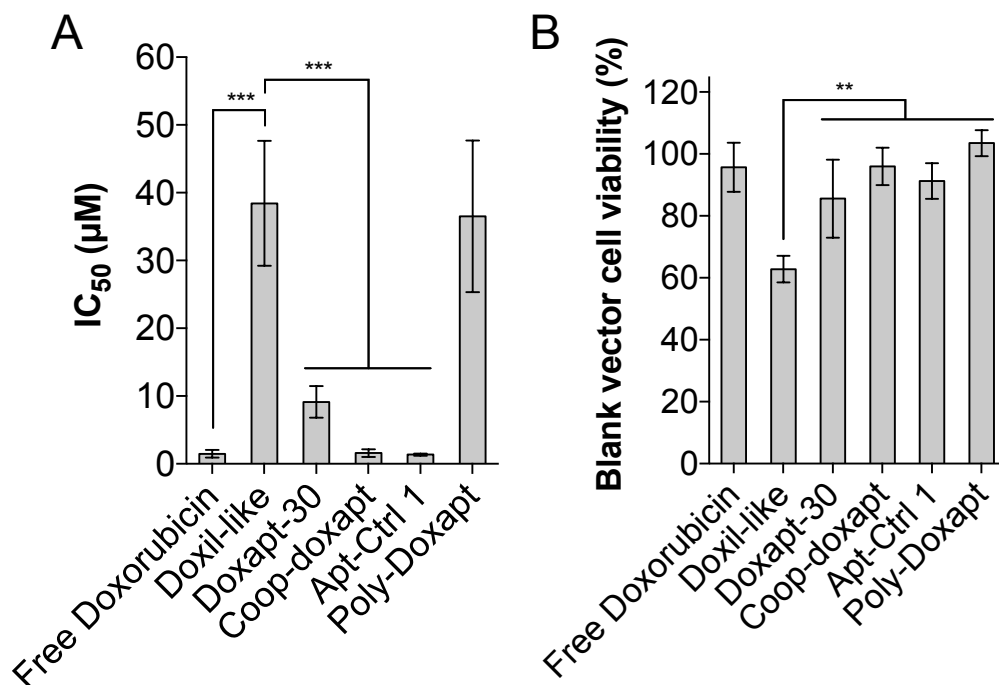
575 Figure 3. Optimization of doxorubicin loading into aptamer-loaded lipoplexes. A) Doxorubicin
 576 encapsulation efficiency (%; bar charts, left) and final Drug/Lipid (D/L) ratio (w/w, dot plot, right)
 577 of Doxapt-30 lipoplexes (N/P = 3) at increasing molar ratios of doxorubicin/aptamer. ‘No apta’
 578 control consisted of the cationic liposome (DOTAP/Chol/DSPE-PEG₂₀₀₀ 50/48/2 molar ratio)
 579 without any DNA. Apt-Ctrl-1 and Apt-Ctrl-2 were assessed at N/P = 3 and Doxorubicin/aptamer
 580 = 2. ‘No cationic lipid’ is a liposome of POPC/Cholesterol/DSPE-PEG₂₀₀₀ 55/40/5 representative
 581 of a neutral formulation for passive encapsulation, tested at D/L = 0.086. Doxil-Like liposome was
 582 assessed at a D/L = 0.1. B) Encapsulation efficiency of doxorubicin within all aptamer-loaded
 583 lipoplexes. For each aptamer, N/P ratio was selected according to the optimized formulation (Table
 584 3): N/P = 2 for Poly-Doxapt and Coop-Doxapt. N/P = 3 for Doxapt-28 and Doxapt-30. Results are
 585 reported as the mean value of 3 experiments, ± standard deviation of the mean.

586

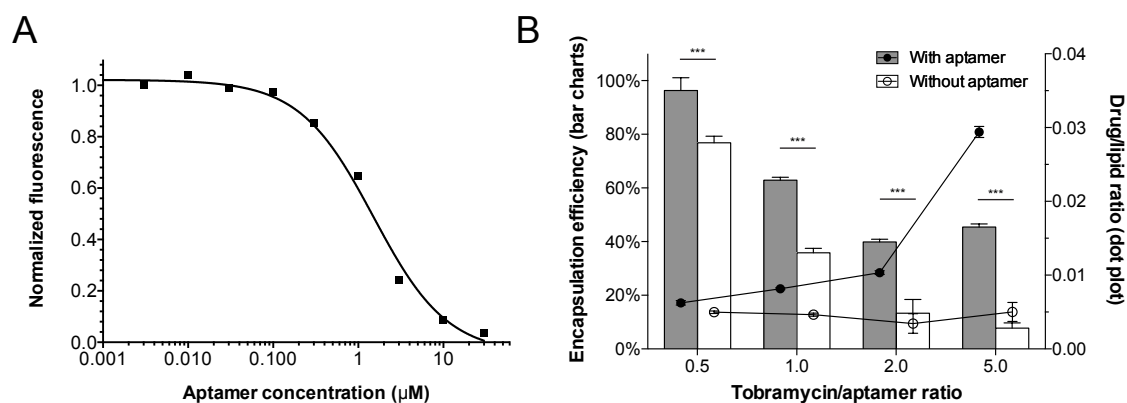


587

588 Figure 4. Release of doxorubicin at 37 °C in PBS (pH 7.4) from optimized formulations of
589 doxorubicin-loaded lipoplexes (see Table 3). 'Free Dox' corresponds to the initial amount of
590 doxorubicin (1 mL of 15 µM doxorubicin) placed in the dialysis bag. Results are reported as the
591 mean value of 3 experiments, ± standard deviation of the mean.



593
 594 Figure 5. Cytotoxic activity of doxorubicin in optimized formulations (see Table 3) on HeLa
 595 cells. A) IC₅₀ values of doxorubicin in optimized formulations after 48h. B) Cell viability of
 596 aptamer-loaded lipoplexes without doxorubicin at their highest concentration used for IC₅₀ assay
 597 (corresponding to 25 µM doxorubicin). Results are reported as the mean value of 3 experiments,
 598 ± standard deviation of the mean. *** P ≤ 0.05.
 599
 600



601
 602 Figure 6. Tobramycin encapsulation using aptamers. A) Binding affinity of Apt-Ctrl-1 for
 603 Tobramycin-Cy5. $K_D = 1.15 \pm 24 \mu\text{M}$. B) Tobramycin encapsulation efficiency (% bar charts,
 604 left) and final Drug/Lipid ratio (w/w, dot plot, right) of aptamer-loaded lipoplexes
 605 (DOTAP/Chol/DSPE-PEG₂₀₀₀ 50/48/2 molar ratio, aptamer Ctrl-1, N/P = 3). Results are reported
 606 as the mean value of 3 experiments, ± standard deviation of the mean. *** P ≤ 0.05.
 607
 608

609
610
611

612
613 [1] A.D. Keefe, S. Pai, A. Ellington, Aptamers as therapeutics, *Nat. Rev. Drug Discov.*, 9 (2010) 537-550.
614 [2] K.E. Maier, M. Levy, From selection hits to clinical leads: progress in aptamer discovery, *Mol. Ther.*
615 *Methods Clin. Dev.*, 5 (2016) 16014.
616 [3] G. Zhu, M. Ye, M.J. Donovan, E. Song, Z. Zhao, W. Tan, Nucleic acid aptamers: an emerging frontier in
617 cancer therapy, *Chem. Commun.*, 48 (2012) 10472-10480.
618 [4] K.-i. Matsunaga, M. Kimoto, C. Hanson, M. Sanford, H.A. Young, I. Hirao, Architecture of high-affinity
619 unnatural-base DNA aptamers toward pharmaceutical applications, *Sci. Rep.*, 5 (2015) 18478.
620 [5] H. Sun, X. Zhu, P.Y. Lu, R.R. Rosato, W. Tan, Y. Zu, Oligonucleotide aptamers: new tools for targeted
621 cancer therapy, *Mol. Ther. Nucleic Acids*, 3 (2014) e182.
622 [6] P.R. Bouchard, R.M. Hutabarat, K.M. Thompson, Discovery and development of therapeutic aptamers,
623 *Annu. Rev. Pharmacol. Toxicol.*, 50 (2010) 237-257.
624 [7] Z. Liu, Y. Lu, Y. Pu, J. Liu, B. Liu, B. Yu, K. Chen, T. Fu, C.J. Yang, H. Liu, W. Tan, Using aptamers to
625 elucidate esophageal cancer clinical samples, *Sci. Rep.*, 5 (2015) 18516.
626 [8] D. Oberthur, J. Achenbach, A. Gabdulkhakov, K. Buchner, C. Maasch, S. Falke, D. Rehders, S. Klussmann,
627 C. Betzel, Crystal structure of a mirror-image L-RNA aptamer (Spiegelmer) in complex with the natural L-
628 protein target CCL2, *Nat. Commun.*, 6 (2015) 6923.
629 [9] Z. Zeng, C.-H. Tung, Y. Zu, A Cancer Cell-Activatable Aptamer-Reporter System for One-Step Assay of
630 Circulating Tumor Cells, *Mol. Ther. Nucleic Acids*, 3 (2014) e184.
631 [10] A. Shastri, L.M. McGregor, Y. Liu, V. Harris, H. Nan, M. Mujica, Y. Vasquez, A. Bhattacharya, Y. Ma, M.
632 Aizenberg, O. Kuksenok, A.C. Balazs, J. Aizenberg, X. He, An aptamer-functionalized chemomechanically
633 modulated biomolecule catch-and-release system, *Nat. Chem.*, 7 (2015) 447-454.
634 [11] B.C. Wengerter, J.A. Katakowski, J.M. Rosenberg, C.G. Park, S.C. Almo, D. Palliser, M. Levy, Aptamer-
635 targeted antigen delivery, *Mol. Ther.*, 22 (2014) 1375-1387.
636 [12] B.S. Ferguson, D.A. Hoggarth, D. Maliniak, K. Ploense, R.J. White, N. Woodward, K. Hsieh, A.J. Bonham,
637 M. Eisenstein, T.E. Kippin, K.W. Plaxco, H.T. Soh, Real-time, aptamer-based tracking of circulating
638 therapeutic agents in living animals, *Sci Transl Med*, 5 (2013) 213ra165.
639 [13] H. Zhang, Y. Ma, Y. Xie, Y. An, Y. Huang, Z. Zhu, C.J. Yang, A controllable aptamer-based self-assembled
640 DNA dendrimer for high affinity targeting, bioimaging and drug delivery, *Sci. Rep.*, 5 (2015) 10099.
641 [14] O.C. Farokhzad, J. Cheng, B.A. Teply, I. Sherifi, S. Jon, P.W. Kantoff, J.P. Richie, R. Langer, Targeted
642 nanoparticle-aptamer bioconjugates for cancer chemotherapy in vivo, *Proc. Natl. Acad. Sci. U. S. A.*, 103
643 (2006) 6315-6320.
644 [15] Y.-H. Lao, K.K.L. Phua, K.W. Leong, Aptamer nanomedicine for cancer therapeutics: barriers and
645 potential for translation, *ACS Nano*, 9 (2015) 2235-2254.
646 [16] J. Liao, B. Liu, J. Liu, J. Zhang, K. Chen, H. Liu, Cell-specific aptamers and their conjugation with
647 nanomaterials for targeted drug delivery, *Exp. Op. Drug Deliv.*, 12 (2014) 493-506.
648 [17] K. Park, Facing the truth about nanotechnology in drug delivery, *ACS Nano*, 7 (2013) 7442-7447.
649 [18] J.V. Natarajan, C. Nugraha, X.W. Ng, S. Venkatraman, Sustained-release from nanocarriers: a review,
650 *J. Control. Release*, 193 (2014) 122-138.
651 [19] J.O. Eloy, M. Claro de Souza, R. Petrilli, J.P. Barcellos, R.J. Lee, J.M. Marchetti, Liposomes as carriers
652 of hydrophilic small molecule drugs: strategies to enhance encapsulation and delivery, *Colloids Surf B*
653 *Biointerfaces*, 123 (2014) 345-363.
654 [20] T.M. Allen, P.R. Cullis, Liposomal drug delivery systems: From concept to clinical applications, *Adv.*
655 *Drug Del. Rev.*, 65 (2013) 36-48.
656 [21] Y. Barenholz, Relevancy of drug loading to liposomal formulation therapeutic efficacy, *J. Liposome*
657 *Res.*, 13 (2003) 1-8.
658 [22] Y. Barenholz, Doxil® — The first FDA-approved nano-drug: Lessons learned, *J. Control. Release*, 160
659 (2012) 117-134.

660 [23] S. Bandak, D. Goren, A. Horowitz, D. Tzemach, A. Gabizon, Pharmacological studies of cisplatin
661 encapsulated in long-circulating liposomes in mouse tumor models, *Anticancer. Drugs*, 10 (1999) 911-920.
662 [24] E. Oude Blenke, E. Mastrobattista, R.M. Schiffelers, Strategies for triggered drug release from tumor
663 targeted liposomes, *Exp. Op. Drug Deliv.*, 10 (2013) 1399-1410.
664 [25] R. Mo, T. Jiang, R. DiSanto, W. Tai, Z. Gu, ATP-triggered anticancer drug delivery, *Nat. Commun.*, 5
665 (2014).
666 [26] R. Mo, T. Jiang, Z. Gu, Enhanced anticancer efficacy by ATP-mediated liposomal drug delivery, *Angew.
667 Chem. Int. Ed.*, 53 (2014) 5815-5820.
668 [27] R. Mo, T. Jiang, W. Sun, Z. Gu, ATP-responsive DNA-graphene hybrid nanoaggregates for anticancer
669 drug delivery, *Biomaterials*, 50 (2015) 67-74.
670 [28] W.-C. Liao, C.-H. Lu, R. Hartmann, F. Wang, Y.S. Sohn, W.J. Parak, I. Willner, Adenosine triphosphate-
671 triggered release of macromolecular and nanoparticle loads from aptamer/DNA-cross-linked
672 microcapsules, *ACS Nano*, 9 (2015) 9078-9086.
673 [29] M.R. Battig, B. Soontornworajit, Y. Wang, Programmable release of multiple protein drugs from
674 aptamer-functionalized hydrogels via nucleic acid hybridization, *J. Am. Chem. Soc.*, 134 (2012) 12410-
675 12413.
676 [30] B. Soontornworajit, J. Zhou, M.P. Snipes, M.R. Battig, Y. Wang, Affinity hydrogels for controlled
677 protein release using nucleic acid aptamers and complementary oligonucleotides, *Biomaterials*, 32 (2011)
678 6839-6849.
679 [31] G. Zhu, J. Zheng, E. Song, M. Donovan, K. Zhang, C. Liu, W. Tan, Self-assembled, aptamer-tethered
680 DNA nanotrains for targeted transport of molecular drugs in cancer theranostics, *Proc. Natl. Acad. Sci. U.
681 S. A.*, 110 (2013) 7998-8003.
682 [32] O. Boyacioglu, C.H. Stuart, G. Kulik, W.H. Gmeiner, Dimeric DNA aptamer complexes for high-capacity-
683 targeted drug delivery using pH-sensitive covalent linkages, *Mol. Ther. Nucleic Acids*, 2 (2013) e107.
684 [33] A.J. Simon, A. Vallée-Bélisle, F. Ricci, K.W. Plaxco, Intrinsic disorder as a generalizable strategy for the
685 rational design of highly responsive, allosterically cooperative receptors, *Proc. Natl. Acad. Sci. U. S. A.*, 111
686 (2014) 15048-15053.
687 [34] P. Sundaram, J. Wower, M.E. Byrne, A nanoscale drug delivery carrier using nucleic acid aptamers for
688 extended release of therapeutic, *Nanomed. Nanotechnol. Biol. Med.*, 8 (2012) 1143-1151.
689 [35] Z. Wu, L.-J. Tang, X.-B. Zhang, J.-H. Jiang, W. Tan, Aptamer-modified nanodrug delivery systems, *ACS
690 Nano*, 5 (2011) 7696-7699.
691 [36] A. Wochner, M. Menger, D. Orgel, B. Cech, M. Rimmelé, V.A. Erdmann, J. Glöckler, A DNA aptamer
692 with high affinity and specificity for therapeutic anthracyclines, *Anal. Biochem.*, 373 (2008) 34-42.
693 [37] V. Bagalkot, O.C. Farokhzad, R. Langer, S. Jon, An aptamer-doxorubicin physical conjugate as a novel
694 targeted drug-delivery platform, *Angew Chem Int Ed Engl*, 45 (2006) 8149-8152.
695 [38] M.-G. Kim, J.Y. Park, W. Miao, J. Lee, Y.-K. Oh, Polyaptamer DNA nanothread-anchored, reduced
696 graphene oxide nanosheets for targeted delivery, *Biomaterials*, 48 (2015) 129-136.
697 [39] K.-M. Song, M. Cho, H. Jo, K. Min, S.H. Jeon, T. Kim, M.S. Han, J.K. Ku, C. Ban, Gold nanoparticle-based
698 colorimetric detection of kanamycin using a DNA aptamer, *Anal. Biochem.*, 415 (2011) 175-181.
699 [40] A.J. Simon, A. Vallée-Bélisle, F. Ricci, H.M. Watkins, K.W. Plaxco, Using the Population-Shift
700 Mechanism to Rationally Introduce "Hill-type" Cooperativity into a Normally Non-Cooperative Receptor,
701 *Angew. Chem. Int. Ed.*, 53 (2014) 9471-9475.
702 [41] H. Yin, R.L. Kanasty, A.A. Eltoukhy, A.J. Vegas, J.R. Dorkin, D.G. Anderson, Non-viral vectors for gene-
703 based therapy, *Nat. Rev. Genet.*, 15 (2014) 541-555.
704 [42] A. Porchetta, A. Vallée-Bélisle, K.W. Plaxco, F. Ricci, Using distal-site mutations and allosteric
705 inhibition to tune, extend, and narrow the useful dynamic range of aptamer-based sensors, *J. Am. Chem.
706 Soc.*, 134 (2012) 20601-20604.

- 707 [43] M.J.H. Janssen, D.J.A. Crommelin, G. Storm, A. Hulshoff, Doxorubicin decomposition on storage.
708 Effect of pH, type of buffer and liposome encapsulation, *Int. J. Pharm.*, 23 (1985) 1-11.
- 709 [44] D.C. Wu, C.M. Ofner, Adsorption and Degradation of Doxorubicin from Aqueous Solution in
710 Polypropylene Containers, *AAPS PharmSciTech*, 14 (2013) 74-77.
- 711 [45] L. Silverman, Y. Barenholz, In vitro experiments showing enhanced release of doxorubicin from Doxil®
712 in the presence of ammonia may explain drug release at tumor site, *Nanomed. Nanotechnol. Biol. Med.*,
713 11 (2015) 1841-1850.
- 714 [46] J. Yu, X. Xie, M. Zheng, L. Yu, L. Zhang, J. Zhao, D. Jiang, X. Che, Fabrication and characterization of
715 nuclear localization signal-conjugated glycol chitosan micelles for improving the nuclear delivery of
716 doxorubicin, *Int. J. Nanomed.*, 7 (2012) 5079-5090.
- 717 [47] T. Fröhlich, D. Edinger, V. Russ, E. Wagner, Stabilization of polyplexes via polymer crosslinking for
718 efficient siRNA delivery, *Eur. J. Pharm. Sci.*, 47 (2012) 914-920.
- 719 [48] J.F. Marier, J.L. Brazier, J. Lavigne, M.P. Ducharme, Liposomal tobramycin against pulmonary
720 infections of *Pseudomonas aeruginosa*: a pharmacokinetic and efficacy study following single and multiple
721 intratracheal administrations in rats, *J. Antimicrob. Chemother.*, 52 (2003) 247-252.
- 722 [49] A.-S. Messiaen, K. Forier, H. Nelis, K. Braeckmans, T. Coenye, Transport of nanoparticles and
723 tobramycin-loaded liposomes in *Burkholderia cepacia* complex biofilms, *PLoS One*, 8 (2013) e79220.
- 724 [50] L. Desigaux, M. Sainlos, O. Lambert, R. Chevre, E. Letrou-Bonneval, J.-P. Vigneron, P. Lehn, J.-M. Lehn,
725 B. Pitard, Self-assembled lamellar complexes of siRNA with lipidic aminoglycoside derivatives promote
726 efficient siRNA delivery and interference, *Proc. Natl. Acad. Sci. U. S. A.*, 104 (2007) 16534-16539.
- 727 [51] N.F. Boussein, C.S. McAllister, K.K. Ewert, C.E. Samuel, C.R. Safinya, Structure and gene silencing
728 activities of monovalent and pentavalent cationic lipid vectors complexed with siRNA, *Biochemistry*, 46
729 (2007) 4785-4792.

730

731